

Atomic-Scale Ru Anchored on Chromium-Shavings as Precursor for pH-Universal Hydrogen Evolution Reaction Electrocatalyst

Qingxin Han^{a##*}, Qiangqiang Lu^{a#}, Xuechuan Wang^{a,b}, Chao Wei^a, Xiaoyu Guan^{a*}, Luming Chen^a,
Xiao Wang^a, & Ji Li^{a*}

^a College of Bioresources Chemical and Materials Engineering, Shaanxi University of Science & Technology, Xi'an 710021, Shaanxi, China

^b Key Laboratory of Auxiliary Chemistry and Technology for Chemical Industry, Ministry of Education & Shaanxi Collaborative Innovation Center of Industrial Auxiliary Chemistry and Technology, Shaanxi University of Science and Technology, Xi'an, 710021, China

[#]These authors contributed to the work equally and should be regarded as co-first authors.

*E-mail: hanqingxin@sust.edu.cn

*E-mail: xiaoyu.guan@riken.jp

*E-mail: lijilj@sust.edu.cn

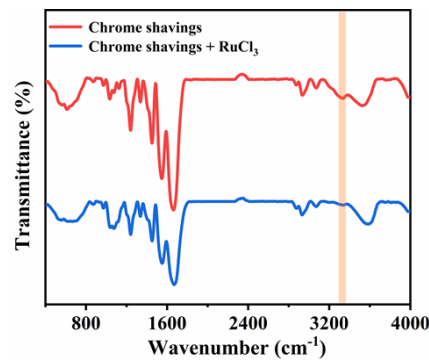


Fig. S1. FT-IR spectra of chrome shavings and chrome shavings were loaded with RuCl₃.

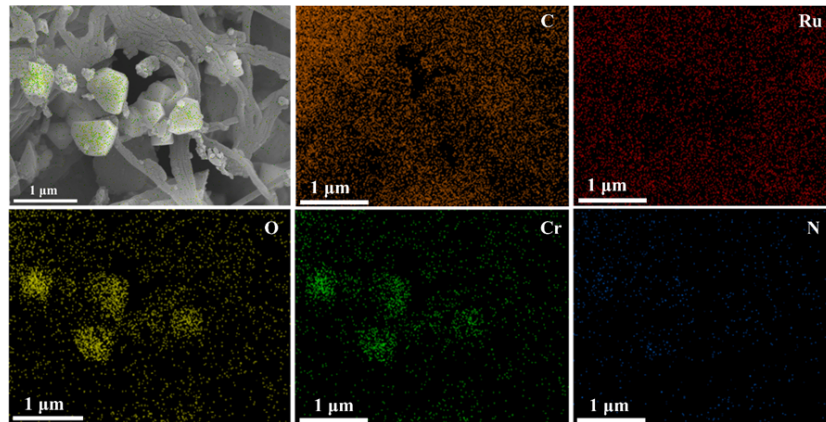


Fig. S2. SEM image and corresponding EDX elemental mapping of C, Ru, O, Cr and N.

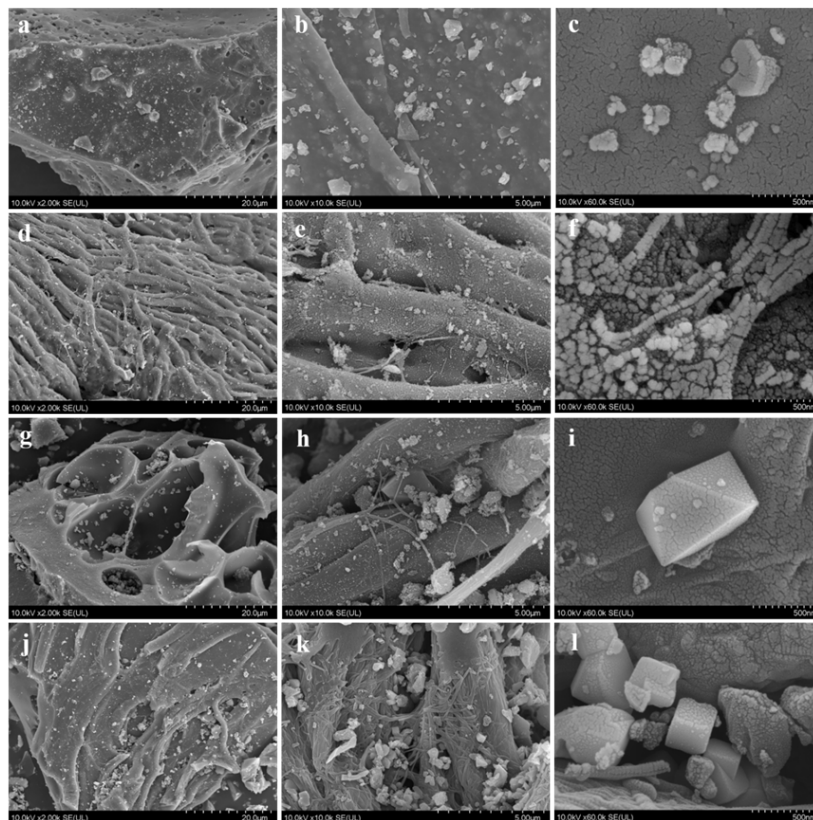


Fig. S3. (a-c) SEM image of CN/Ru-1; (d-f) SEM of CN/Cr₂O₃/Ru-0.1; (g-i) SEM of CN/Cr₂O₃/Ru-5; (j-l) SEM of CN/Cr₂O₃/Ru-10.

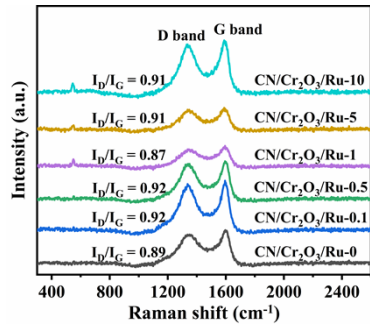


Fig. S4. Raman spectra of catalyst samples.

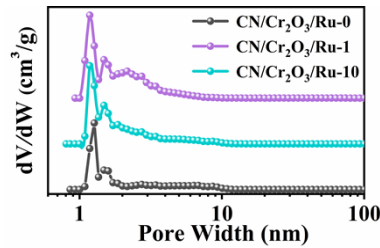


Fig. S5. Pore size distribution of the sample.

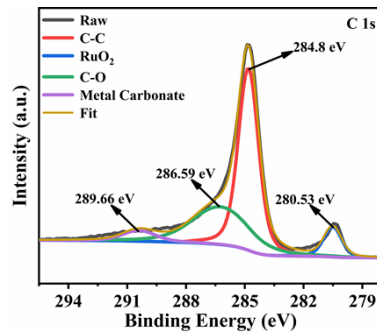


Fig. S6. XPS of CN/Cr₂O₃/Ru-1 for C 1s regions.

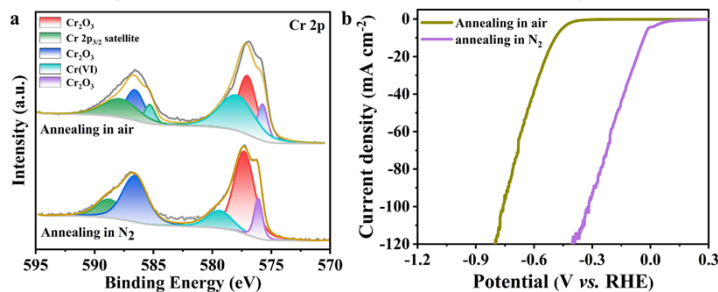


Fig. S7. (a) The change of Cr (VI) content is in Cr 2p; (b) Comparison of LCV curves with different Cr (VI) contents.

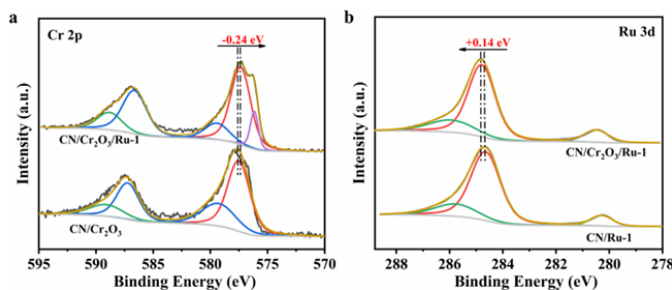


Fig. S8. The changes of Cr 2p (a) and Ru 3d (b) orbitals of CN/Cr₂O₃/Ru-1 and CN/Ru-1, CN/Cr₂O₃.

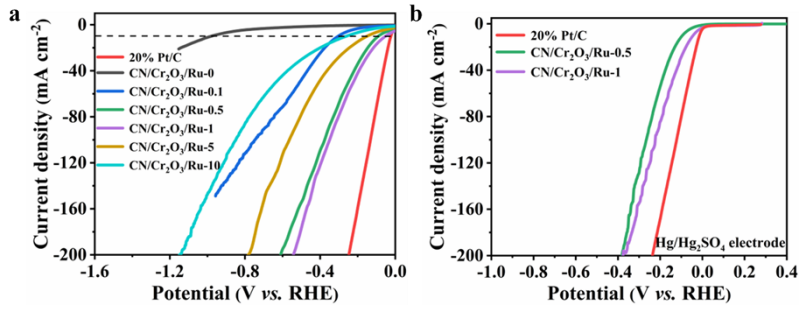


Fig. S9. (a) LSV polarization curves of CN/Cr₂O₃/Ru-0, CN/Cr₂O₃/Ru-0.1, CN/Cr₂O₃/Ru-0.5, CN/Cr₂O₃/Ru-1, CN/Cr₂O₃/Ru-5, CN/Cr₂O₃/Ru-10 and 20% Pt/C catalysts in 1.0 M H₂SO₄; (b) LSV polarization curves of CN/Cr₂O₃/Ru-0.5, CN/Cr₂O₃/Ru-1 and 20% Pt/C catalysts in Hg/Hg₂SO₄ electrode.

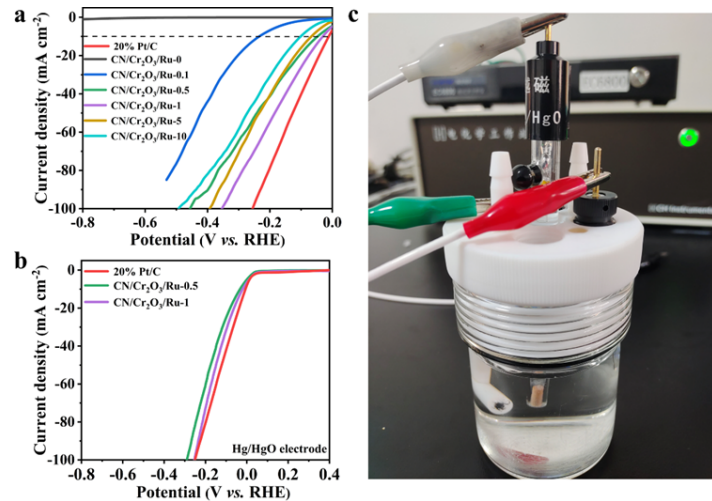


Fig. S10. (a) LSV polarization curves of CN/Cr₂O₃/Ru-0, CN/Cr₂O₃/Ru-0.1, CN/Cr₂O₃/Ru-0.5, CN/Cr₂O₃/Ru-1, CN/Cr₂O₃/Ru-5, CN/Cr₂O₃/Ru-10 and 20% Pt/C catalysts in 1.0 M KOH; (b) LSV polarization curves of CN/Cr₂O₃/Ru-0.5, CN/Cr₂O₃/Ru-1 and 20% Pt/C catalysts in Hg/HgO electrode; (c) Real test scenarios.

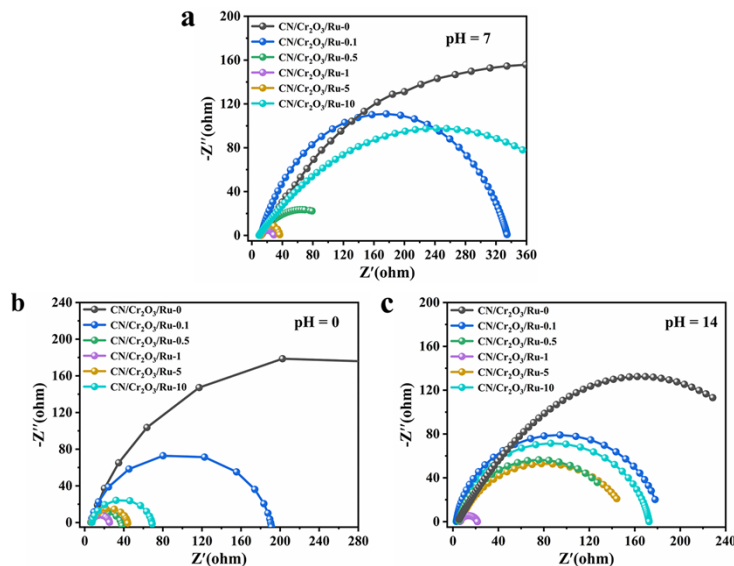


Fig. S11. Nyquist plots of CN/Cr₂O₃/Ru-0, CN/Cr₂O₃/Ru-0.1, CN/Cr₂O₃/Ru-0.5, CN/Cr₂O₃/Ru-1, CN/Cr₂O₃/Ru-5 and CN/Cr₂O₃/Ru-10 in (a) 1.0 M PBS, (b) 0.5 M H₂SO₄ and (c) 1.0 M KOH.

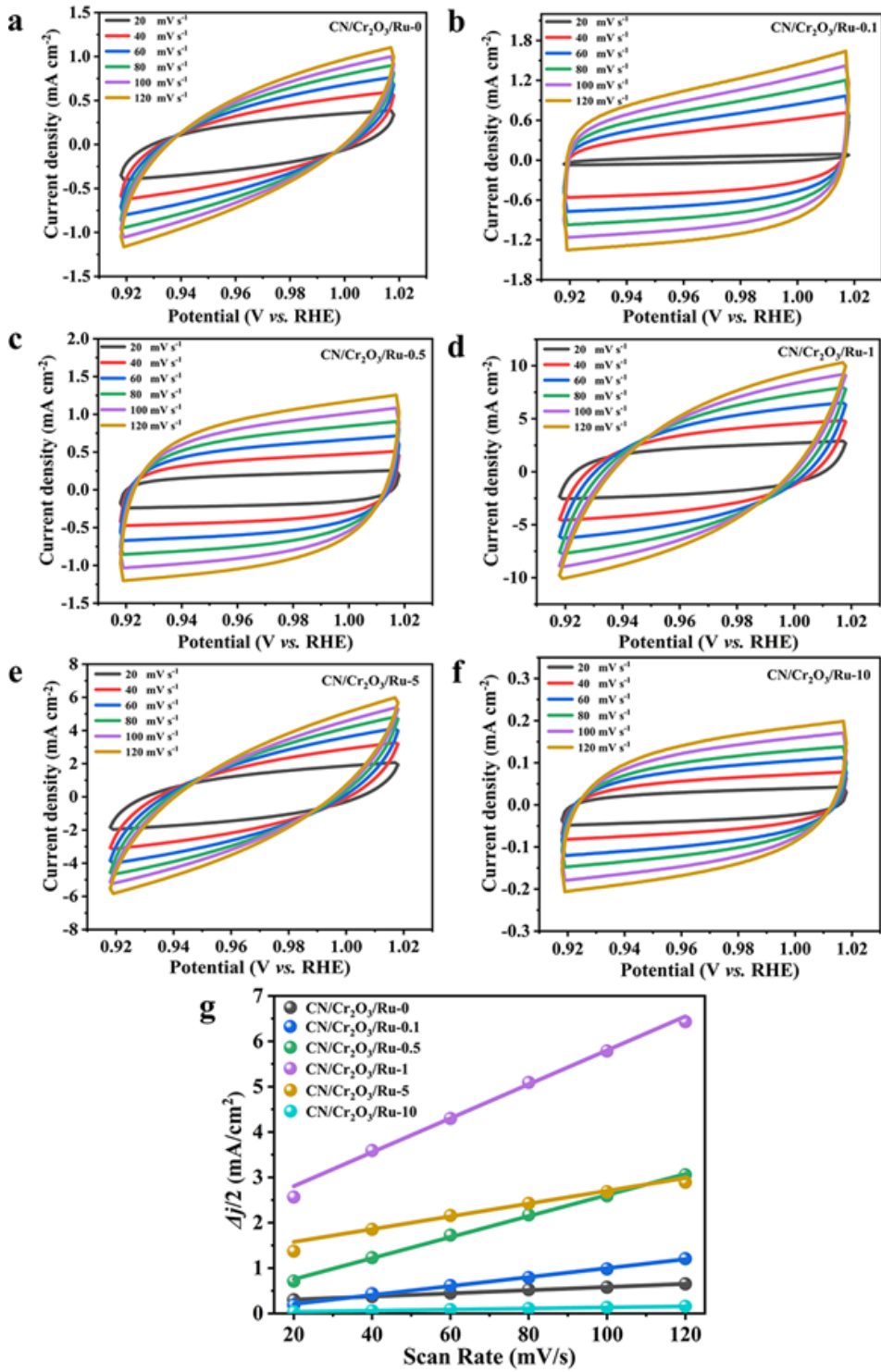


Fig. S12. (a-f) CV curves obtained in a potential window of 0.092–0.192 V (vs. RHE) at different scan rates in 1.0 M KOH for CN/Cr₃O_y/Ru-0, CN/Cr₃O_y/Ru-0.1, CN/Cr₂O₃/Ru-0.5, CN/Cr₂O₃/Ru-1, CN/Cr₂O₃/Ru-5 and CN/Cr₂O₃/Ru-10, respectively. (g) Charging current density plots with different scan rates for the samples.

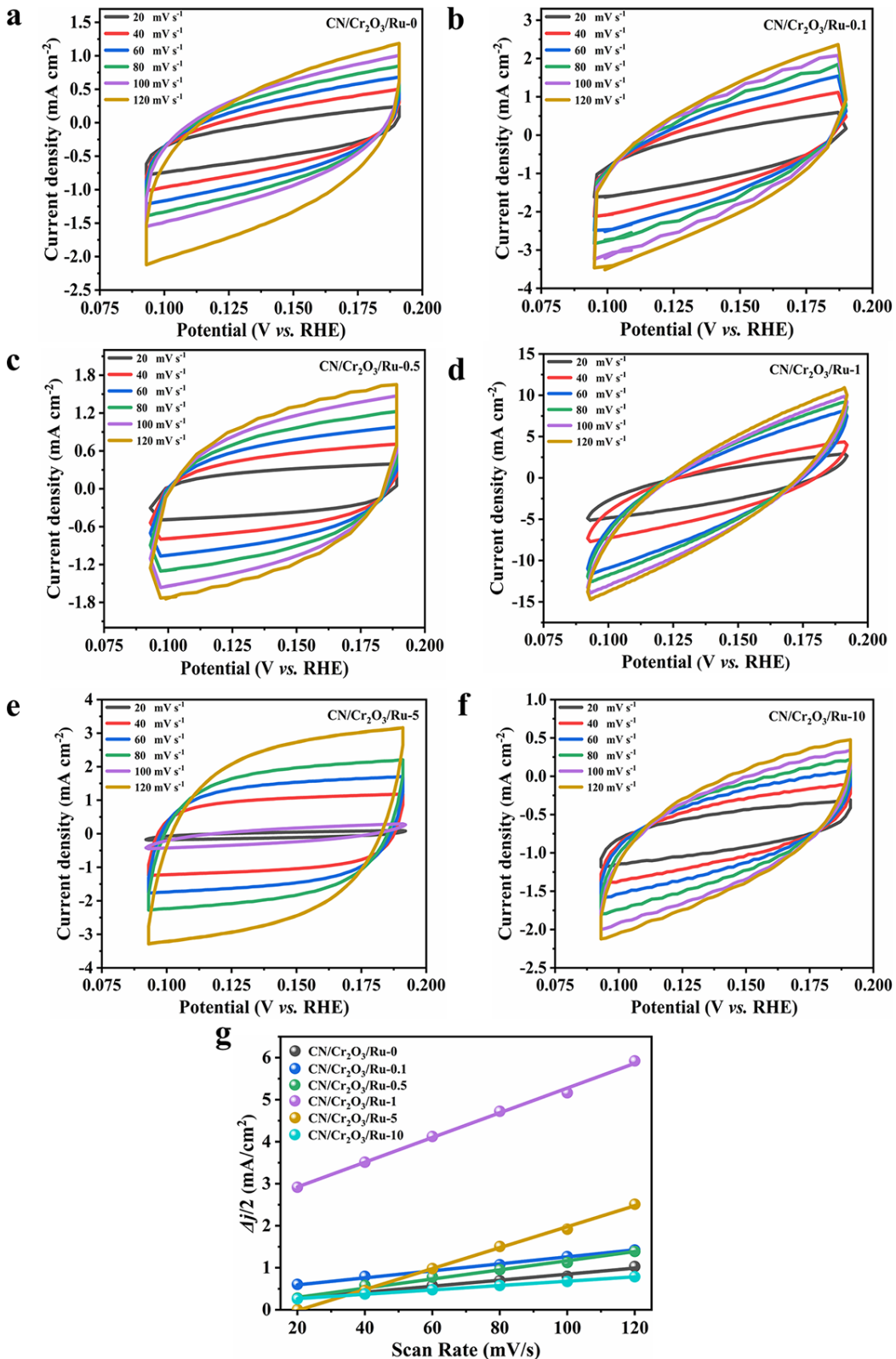


Fig. S13. (a-f) CV curves obtained in a potential window of 0.092-0.192 V (vs. RHE) at different scan rates in 0.5 M H_2SO_4 for $\text{CN/Cr}_2\text{O}_3/\text{Ru-0}$, $\text{CN/Cr}_2\text{O}_3/\text{Ru-0.1}$, $\text{CN/Cr}_2\text{O}_3/\text{Ru-0.5}$, $\text{CN/Cr}_2\text{O}_3/\text{Ru-1}$, $\text{CN/Cr}_2\text{O}_3/\text{Ru-5}$ and $\text{CN/Cr}_2\text{O}_3/\text{Ru-10}$, respectively. (g) Charging current density plots with different scan rates for the samples.

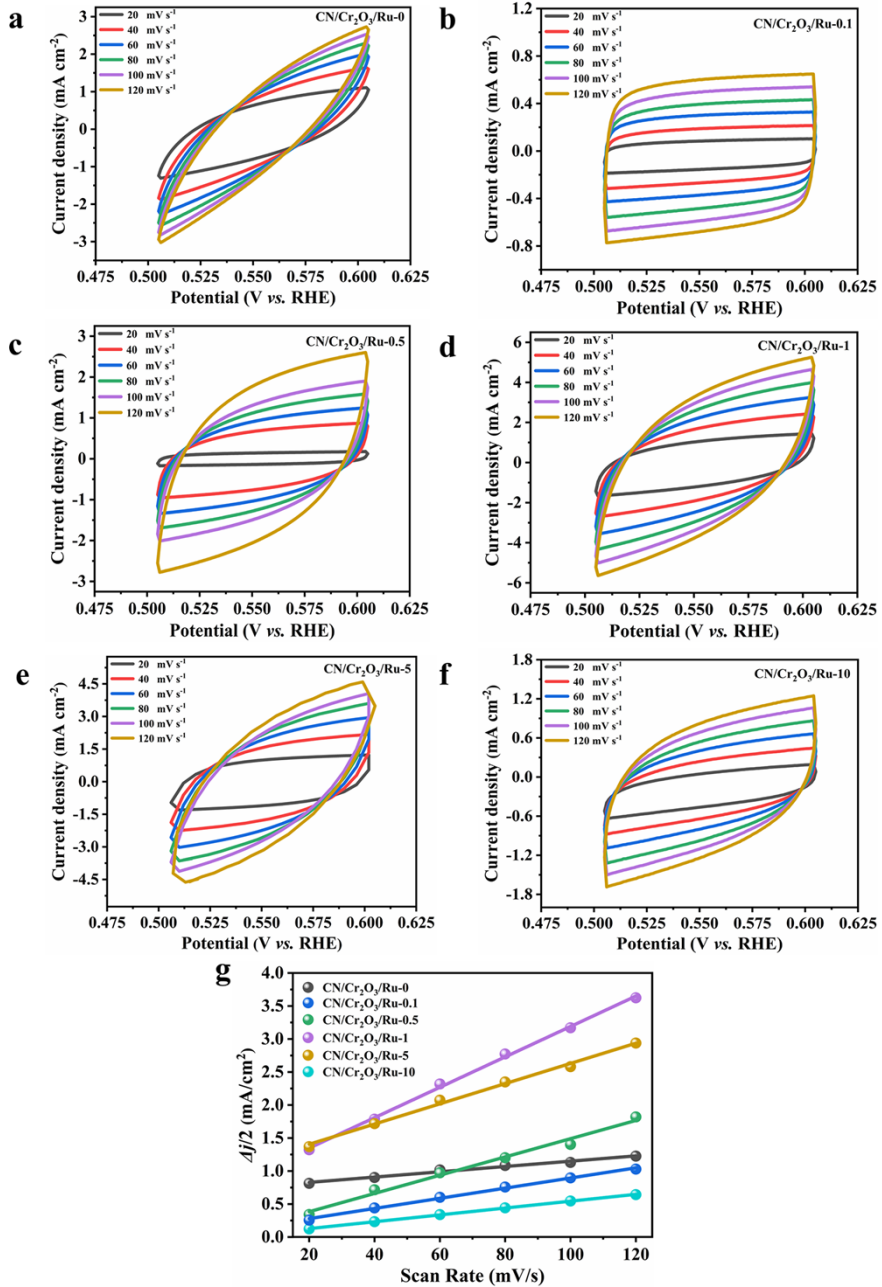


Fig. S14. (a-f) CV curves obtained in a potential window of 0.092–0.192 V (vs. RHE) at different scan rates in 1.0 M PBS for CN/Cr₂O₃/Ru-0, CN/Cr₂O₃/Ru-0.1, CN/Cr₂O₃/Ru-0.5, CN/Cr₂O₃/Ru-1, CN/Cr₂O₃/Ru-5 and CN/Cr₂O₃/Ru-10, respectively. (g) Charging current density plots with different scan rates for the samples.

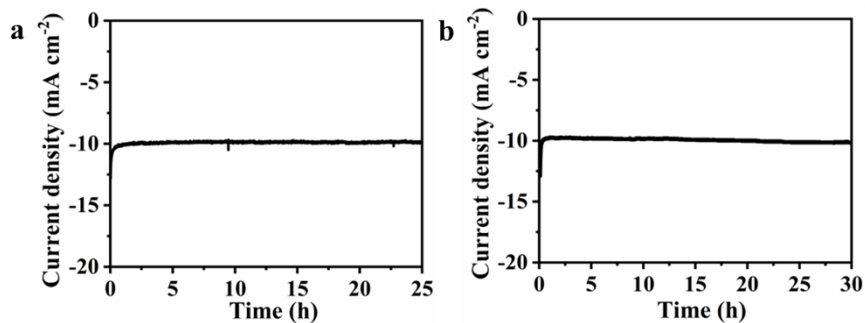


Fig. S15. HER stability (i-t curves) of CN/Cr₂O₃/Ru-1 in (a) 0.5 M H₂SO₄, (b) 1.0 M PBS.

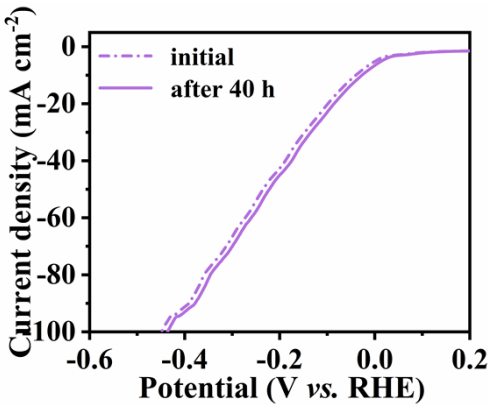


Fig. S16. the LSV curves before and after the durability test.

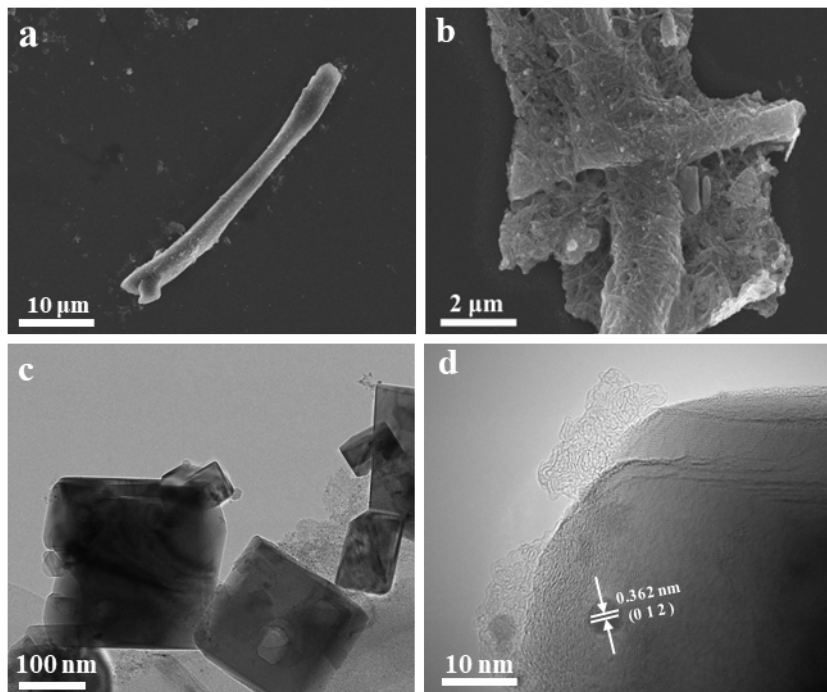


Fig. S17. (a) and (b) SEM images of CN/Cr₂O₃/Ru-1 after the durability test in 1.0 M KOH.

(c) and (d) SEM images of CN/Cr₂O₃/Ru-1 after the durability test in 1.0 M KOH.

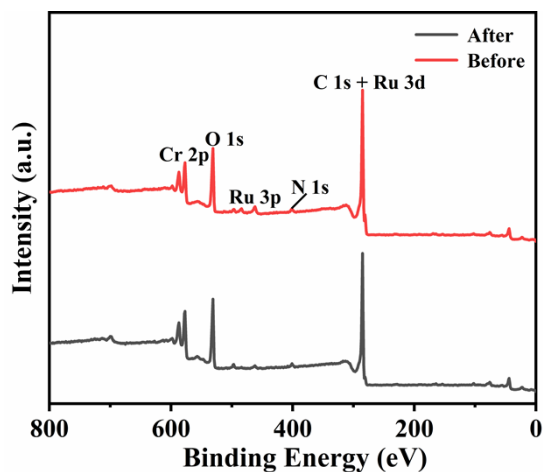


Fig. S18. XPS survey spectra of CN/Cr₂O₃/Ru-1 before and after stability test in 1.0 M KOH.

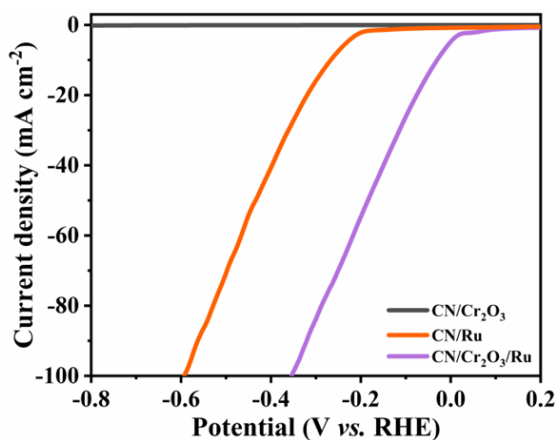


Fig. S19. Comparison of HER performance of three catalysts.

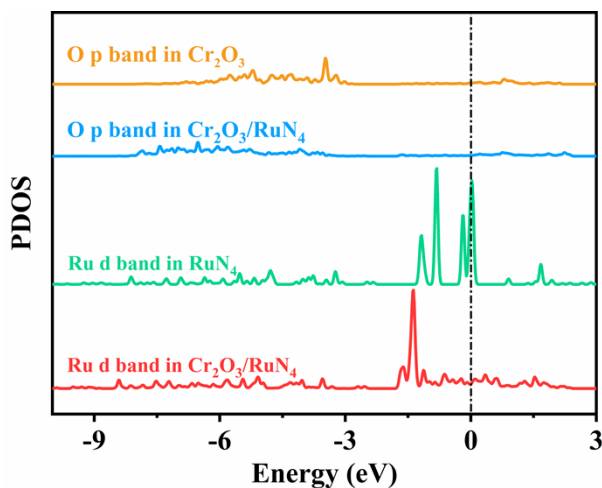


Fig. S20. Calculated PDOS of Cr_2O_3 , $\text{Cr}_2\text{O}_3/\text{RuN}_4$, RuN_4 .

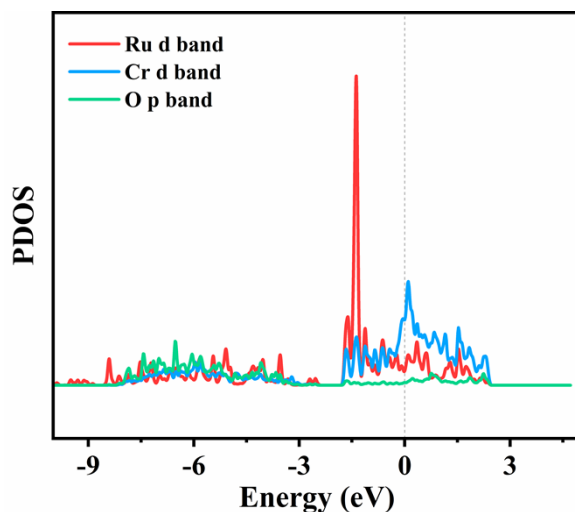


Fig. S21. PDOS of Ru d band, Cr d band and O p band electrons.

Table S1. Elemental contents (wt%) detected by XPS.

Samples	$S_{\text{BET}} (\text{m}^2 \text{ g}^{-1})$	Pore volumes ($\text{cm}^3 \text{ g}^{-1}$)
CN/ Cr_2O_3 -0	332.5	0.25
CN/ Cr_2O_3 -1	843.8	0.49
CN/ Cr_2O_3 -10	518.8	0.33

Table S2. Elemental contents (wt%) detected by XPS.

Samples	C	N	O	Cr	Ru
CN/Cr ₂ O ₃ /Ru-0	84.46	2.25	11.51	1.78	0
CN/Cr ₂ O ₃ /Ru-0.1	77.33	2.41	16.49	3.27	0.5
CN/Cr ₂ O ₃ /Ru-0.5	82.1	1.93	11.93	2.97	1.07
CN/Cr ₂ O ₃ /Ru-1	78.64	2.04	13.69	2.9	2.74
CN/Cr ₂ O ₃ /Ru-5	75.33	2.41	14.49	2.27	5.5
CN/Cr ₂ O ₃ /Ru-10	75.96	1.95	10.99	2.15	8.95

Table S3. EXAFS fitting parameters at the Ru K-edge for various samples ($S_0^2=0.78$)

Sample	Shell	CN ^a	R(Å) ^b	$\sigma^2(\text{\AA}^2)$ ^c	$\Delta E_0(\text{eV})$ ^d	R factor
Ru foil	Ru-Ru	12*	2.68±0.01	0.0042	3.8	0.0072
	Ru-O	6.0±0.4	1.96±0.01	0.0015	-3.9	
RuO ₂	Ru-Ru	6.0±0.8	3.12±0.01	0.0072	-8.9	0.0149
	Ru-Ru	6.1±0.3	3.58±0.01	0.0013	2.2	
Ru sample	Ru-C/N	4.0±0.4	2.02±0.01	0.0029	-12.9	
	Ru-Cl	1.8±0.2	2.41±0.01	0.0043	11.7	0.0196
	Ru-Ru	1.0±0.2	2.63±0.01	0.0057	14.7	

^aCN, coordination number; ^bR, distance between absorber and backscatter atoms; ^c σ^2 , Debye-Waller factor to account for both thermal and structural disorders; ^d ΔE_0 , inner potential correction; R factor indicates the goodness of the fit. S_0^2 was fixed to 0.78, according to the experimental EXAFS fit of Ru foil by fixing CN as the known crystallographic value.

Table S4. A comparison of overpotentials (mV) at 10 mA/cm²

Medium	Reference electrode	Pt/C	CN/Cr ₂ O ₃ /Ru-0.5	CN/Cr ₂ O ₃ /Ru-1
1.0 M KOH	Hg/Hg ₂ Cl ₂	12	47	28
	Hg/HgO	11	40	24
0.5 M H ₂ SO ₄	Hg/Hg ₂ Cl ₂	10	96	58
	Hg/Hg ₂ SO ₄	14	97	47

Table S5. ICP-OES analysis of dissolved Ru and Cr ions after stability test in 1.0 M KOH.

Sample amount	2 mg	4 mg	5 mg
Concentration of Ru ion (ppb)	0.18	0.25	0.49
Concentration of Cr ion (ppb)	0.24	0.45	0.77
Loss of mass (Ru)	3.51%	2.44%	1.91%
Loss of mass (Cr)	4.83%	4.53%	6.2%
Average mass loss (Ru)		2.62%	
Average mass loss (Cr)		5.18%	

Table S6. Comparison of HER performances of Ru-based catalysts.

No.	Catalyst	η_{10} (mV)	Reference
1	Ru SAs/Ru PNs	23	Int. J. Hydrogen Energy. 2020, 18840-18849.
2	RuAu-0.2	24	Adv. Energy Mater. 2019, 9, 1803913.
3	CN/Cr ₂ O ₃ /Ru-1	28	This work
4	RuCo alloy	28	Nat. Commun. 2017, 8, 14969
5	NiRu alloy	32	J. Mater. Chem. A. 2018, 6, 1376-1381.
6	Ru _{NP} -Ru _{SA} @CFN-800	33	Adv. Funct. Mater. 2023, 33, 2213058.
7	Ru SAs/N-Mo ₂ C NSs	43	Appl. Catal. B., 2020, 277, 119236.
8	CoRu@NC	45	Nanotechnology. 2018, 29, 225403.
9	Ru ₂ P@PNC/CC-900	50	ACS Appl. Energy Mater. 2018, 1, 314-3150.
10	Ru _I CoP/CDs-1000	51	Angew. Chem. Int. Ed. 2021, 60, 7234-7244.
11	Ru _{0.10} @2H-MoS ₂	51	Appl. Catal. B-Environ. 2021, 298, 120490.
12	RuP ₂ @NPC	52	Angew. Chem. Int. Ed. 2017, 56, 11559-11564.
13	Ru/Co ₄ N-CoF ₂	53	Chem. Eng. J. 2021, 414, 128865.
14	ah-RuO ₂ @C	63	Nano Energy. 2019, 55, 49-58.
15	CF@Ru-CoCH NWs	66	Electrochim. Acta. 2020, 331, 135367.
16	RuP _x @NPC	74	ChemSusChem. 2018, 11, 743-752.
17	Ru SAs/ECM	83	Adv. Energy Mater. 2020, 10, 2000882.
18	CoRu-O/A@HNC-2	85	ACS Appl. Mater. Interfaces. 2020, 12, 51437-51447.
19	Ru-WSe ₂	87	Inorg. Chem. Front. 2019, 6, 1382-1387.
20	Ru-MoS ₂ /CC	90	NEW J. CHEM. 2022, 46, 1912-1920.
21	Ru NPs/Mo ₂ C NSs	95	Appl. Catal. B. 2020, 277, 119236.
22	RuO ₂ -NWs@g-CN	95	ACS Appl. Mater. Interfaces 2016, 8, 28678-28688.
23	Ru/Y(OH) ₃	100	Chem. Commun. 2018, 54, 12202-12205.
24	SrRuO ₃ /CNT	110	ACS Appl Energy Mater. 2019, 2, 956-960.
25	Ru-VN-2	144	ChemElectroChem. 2020, 7, 1201-1206.

